

BINARY COMPACT OBJECT COALESCENCE RATES: THE ROLE OF ELLIPTICAL GALAXIES

R. O'SHAUGHNESSY

Center for Gravitational Wave Physics, Penn State University, University Park, PA 16802, USA

V. KALOGERA

Northwestern University, Department of Physics and Astronomy, 2145 Sheridan Road, Evanston, IL 60208, USA

AND

KRZYSZTOF BELCZYNSKI^{1,2,3}

¹ Los Alamos National Laboratory, CCS-2/ISR-1 Group

² Oppenheimer Fellow

³ Astronomical Observatory, University of Warsaw, Al. Ujazdowskie 4, 00-478 Warsaw, Poland

Draft version December 15, 2018

ABSTRACT

In this paper we estimate binary compact object merger detection rates for LIGO, including the potentially significant contribution from binaries that are produced in elliptical galaxies near the epoch of peak star formation. Specifically, we convolve hundreds of model realizations of elliptical- and spiral-galaxy population syntheses with a model for elliptical- and spiral-galaxy star formation history as a function of redshift. Our results favor local merger rate densities of $4 \times 10^{-3} \text{ Mpc}^{-3} \text{ Myr}^{-1}$ for binary black holes (BH), $3 \times 10^{-2} \text{ Mpc}^{-3} \text{ Myr}^{-1}$ for binary neutron stars (NS), and $10^{-2} \text{ Mpc}^{-3} \text{ Myr}^{-1}$ for BH-NS binaries. We find that mergers in elliptical galaxies are a significant fraction of our total estimate for BH-BH and BH-NS detection rates; NS-NS detection rates are dominated by the contribution from spiral galaxies. Limiting attention to elliptical- plus only those spiral-galaxy models that reproduce current observations of Galactic NS-NS, we find slightly higher rates for NS-NS and largely similar ranges for BH-NS and BH-BH binaries. Assuming a detection signal-to-noise ratio threshold of 8 for a single detector (in practice as part of a network, to reduce its noise), corresponding to radii D_{bns} of the effective volume inside of which a single LIGO detector could observe the inspiral of two $1.4M_{\odot}$ neutron stars of 14 Mpc and 197 Mpc, for initial and advanced LIGO, we find event rates of *any* merger type of $2.9 \times 10^{-2} - 0.46$ and $25 - 400$ per year (at 90% confidence level), respectively. We also find that the probability P_{detect} of detecting one or more mergers with this single detector can be approximated by (i) $P_{\text{detect}} \simeq 0.4 + 0.5 \log(T/0.01 \text{ yr})$, assuming $D_{\text{bns}} = 197 \text{ Mpc}$ and it operates for T years, for T between 2 days and 0.1 yr; or by (ii) $P_{\text{detect}} \simeq 0.5 + 1.5 \log D_{\text{bns}}/32 \text{ Mpc}$, for one year of operation and for D_{bns} between 20 and 70 Mpc.

Subject headings: Stars: Binaries: Close; Stars: Pulsars: General; Gravitational waves

1. INTRODUCTION

Over the last decade the question of the Galactic inspiral rate of binaries with two compact objects (neutron stars NS or black holes BH) has attracted attention primarily because of the development and planning of gravitational-wave interferometric detectors both on the Earth and in space (e.g., LIGO and GEO600, described in Abbott et al. (The LIGO Scientific Collaboration) (2003); Virgo, described at the Virgo project website www.virgo.infn.it; and LISA, at lisa.nasa.gov). These rate estimates have been widely used in the assessment of gravitational inspiral detectability, given assumed instrument sensitivities. A number of different groups have calculated inspiral rates using population synthesis calculations, most commonly with Monte Carlo methods (Fryer et al. 1998; Portegies Zwart & Yungelson 1998; Brown & Bethe 1994; Fryer et al. 1999; Belczynski et al. 2002;

Voss & Tauris 2003). Such studies consider the complete formation history of double compact objects through long sequences of binary evolution phases, terminated by a gravitational-wave driven inspiral towards merger. Though less critical for studies of the Milky Way, contributions to the present-day merger rate per unit volume from early star formation has most often been ignored in merger rate calculations. Since long inspiral delays before merger are not sufficiently uncommon, even for double neutron stars, merger detection rate calculations should account for the full time history of star formation, including star formation in the early universe; see for example de Freitas Pacheco et al. (2006). Additionally, our current understanding of single and binary star evolution is incomplete. The many uncertainties have been parameterized and the resulting parameter space explored in some studies to determine the range of plausible results (see, e.g., Belczynski et al. 2008b), both by focusing narrowly on physically-motivated regions of parameter space as in Belczynski et al. (2008b) and by broadly exploring all plausible population synthesis simulations (see, e.g.,

Electronic address: oshaughn@gravity.psu.edu

Electronic address: vicky@northwestern.edu

Electronic address: kbelczyn@nmsu.edu

O’Shaughnessy et al. 2008a, and references therein; henceforth denoted PS-GRB). Finally, by assigning equal prior likelihood to any population synthesis model, PS-GRB estimated the relative likelihood of any BH-NS or NS-NS merger rate.¹

The population of binary black holes, however, behaves qualitatively differently from BH-NS or NS-NS binaries: (i) most of those that merge do so only after a few to several Gyr delay after their birth as binary stars; and (ii) those BH-BH binaries with merger times from 1 – 10 Gyr have masses quite different from the typical assumption of a $10M_{\odot}$ BH; see Appendix. The rarity, long delay times, high masses and thus cosmologically significant detection horizons of binary black holes have already been discussed in the literature (see, e.g., Kulczycki et al. (2006) and references therein). However, population synthesis simulations extensive enough to contain a statistically meaningful binary black hole population come at a significant computational cost. Even with adequate population synthesis simulations, given the long-lived nature of the progenitors, BH-BH merger and detection rates depend critically on the earliest and least certain star formation rates. Certain exotic but not exceptionally uncommon binary evolution scenarios could lead to a “high rate tail” – a scenario with rare massive mergers, for example, that could plausibly produce a merger detection in the near future. In this paper we strive to understand what realistic scenarios could lead to a “high rate tail” that LIGO could detect or, conversely, constrain.

Given the technical challenges and significant uncertainties involved, only one paper (O’Shaughnessy et al. 2005) has previously estimated the relative likelihood of different BH-BH detection rate estimates expected from isolated binary star evolution, only for the Milky Way. In the present study we calculate the expected detection rate for LIGO while for the first time simultaneously including (i) all past star formation, particularly the overwhelming importance of elliptical galaxies; (ii) a large database of results that accounts for the dominant model uncertainties; and (iii) a careful treatment of the mass distribution of BH-BH binaries. Additionally, unlike previous analyses presenting distributions of merger rates, we have post-facto varied the birth binary fraction of stars from 100% to 15%; this addition allows us to better compare our results with the fiducial population synthesis model and BH-BH merger rates presented in Belczynski et al. (2007). Finally, whereas previous comparisons relied essentially on confidence intervals (e.g., PS-GRB and O’Shaughnessy et al. (2008b), henceforth denoted PSC2), in this paper we generate true posterior distributions: each model is weighted by its relative conditional likelihood given observations of merging NS-NS binaries in the Milky Way.

To fully assess the *total* probability for a LIGO detection, rather than limit attention to BH-BH mergers we explore the rate at which all LIGO-detectable binaries (BH-BH, BH-NS, and NS-NS; henceforth collectively de-

noted as compact binary coalescences or CBCs) merge through gravitational wave emission. As the methods used to determine LIGO detection rates from population synthesis simulations are already extensively discussed in the literature (see, e.g. Bulik et al. 2004, and PS-GRB), our presentation only reviews those tools, emphasizing unique features of our present analysis (i.e., our methods to estimate BH-BH masses). Specifically, in § 2 we briefly review the ingredients that enter into an estimate of the gravitational wave detection rate for a short-ranged network ($z_{max} \ll 1$). While the local universe is emphasized in the text, networks of advanced ground-based interferometers can detect optimally oriented BH-BH binaries with component masses $M \simeq 10 - 15M_{\odot}$ at cosmologically significant distances $z \geq 0.1$. Merger rates on the past light cone of a detector become inhomogeneous (versus redshift) at this scale, simply because the star formation rate increases dramatically near $z \simeq 1 - 2$ during the epoch of galaxy assembly. At these distances, the detection rate must be integrated over the mass distribution, the full networked orientation-dependent sensitivity, and redshift-dependent merger rate. This integral becomes increasingly sensitive to rare, high-mass events that can be seen in the ancient universe. Therefore, in the Appendix we generalize the short-range method described in § 2 to include all sources on the past light cone, to arbitrary redshift and with accurate orientation-dependent sensitivity. In § 3 we review the model for star formation in the universe adopted here. This experience is applied in § 4 (for BH-BH binaries) and § 5 (including NS-NS and BH-NS binaries too), where we review our population synthesis calculations; and explain what features of those calculations influence our predictions for the relative likelihood of a LIGO detection. These sections also describe Figure 4, which contains our predictions regarding initial and advanced LIGO detection rates. Finally, in § 5.2 we show how rate constraints from the observed sample of Milky Way NS-NS binaries affect the predictions for LIGO detection rates.

To summarize, by fully simulating the past history of the local universe, this paper develops models for the present-day detection rate of short-range ($z \ll 1$; described in the text) and long-range (z not much less than 1; described in the Appendix) gravitational-wave detectors. Our results are rate distributions, where each distribution includes some normalization uncertainties (star formation rate and fraction of stars born in binaries); certain population synthesis model parameters; and our simulation Monte Carlo uncertainty. Further, our Bayesian approach to model constraints surveys many key uncertainties that should be included, whatever the model family involved, when attempting to interpret upper limits or detections from pulsar populations and gravitational wave observatories. We believe our distributions represent the best predictions of a concrete, conservative model family that includes both elliptical and spiral star formation yet is also consistent with initial LIGO upper limits on CBC merger rates.

2. GRAVITATIONAL WAVE DETECTION

This section primarily reviews the final stage in any calculation of a LIGO detection rate: the connection between, on the one hand, the event rate per comoving volume \mathcal{R} and mass distribution $p(m_1, m_2)$

¹ Previously, O’Shaughnessy et al. (2005, 2008b) estimated LIGO binary merger detection rates by extrapolating from the local Milky Way based on the blue light density in the nearby Universe. As we discuss here, their estimate is accurate for short distances and for binary merger progenitors that are not preferentially long-lived (i.e., the median delay between birth and merger is less than 1 Gyr).

of merging binaries and, on the other hand, the detection rate R_D [Eq. (9)]. This relation depends critically on the range to which LIGO could observe each merger. A thorough discussion of the LIGO range requires careful review of data analysis strategies and interferometer network geometry, and remains substantially beyond the scope of this paper. For details see Abbott et al. (The LIGO Scientific Collaboration) (2008); Abbott et al. (The LIGO Scientific Collaboration) (2009) and references therein. For example, with modern multi-mass-region searches using inspiral templates, one essential effect is a merger detection threshold in SNR that changes with total binary mass, as the well-understood portions of detection templates grow shorter. In this paper, we adopt the customary set of approximations (described below) and ignore the errors they introduce.

The distance to which LIGO is sensitive can be calculated using the sensitivity of the detector (strictly, the strain noise spectral distribution S_h), the masses of the inspiralling bodies, and the emitted waveform. [For simplicity, we will assume the black holes initially nonspinning.] Specifically, for a source with masses m_1 and m_2 , merging at a luminosity distance D (or equivalently at redshift z , or comoving distance r) with a binary inclination ι and a relative orientation to the detector given by θ, ϕ (the orientation on the sky) and ψ (a phase angle in the plane of the detector), the signal-to-noise seen by a matched-filter search in the LIGO data stream can be expressed relative to the strain noise spectrum of a single interferometer S_h and the Fourier transform \tilde{h} of gravitational wave strain h received at the detector by an arbitrarily oriented and located source by

$$\rho^2 = 4 \frac{w(\theta, \phi, \psi, \iota)^2}{D^2} \int_0^\infty df \frac{|r\tilde{h}(m_1(1+z), m_2(1+z), f)|^2}{S_h(f)} \quad (1)$$

using units with $G = c = 1$, the known dependence of planar-symmetry gravitational waves on angle, and a standard one-sided Fourier convention for \tilde{h} and S_h . The function $w(\theta, \phi, \psi, \iota)$ takes values between 0 and 1 and completely encompasses the detector- and source-orientation dependent sensitivity for the most common sources, those that are dominated by $l = m = 2$ quadrupole emission²

$$w(\theta, \phi, \psi, \iota) = \sqrt{F_+^2(1 + \cos^2 \iota)^2/4 + F_\times^2 \cos^2 \iota} \quad (2)$$

$$F_+ = \frac{1}{2}(1 + \cos^2 \theta) \cos 2\phi \cos 2\psi + \cos \theta \sin 2\phi \sin 2\psi \quad (3)$$

$$F_\times = -\frac{1}{2}(1 + \cos^2 \theta) \sin 2\phi \cos 2\psi + \cos \theta \cos 2\phi \sin 2\psi \quad (4)$$

To a rough approximation that depends on the data analysis strategy used and the amount of nongaussian noise present in the detector, a single LIGO interferometer can detect the gravitational wave signature of a merging binary if $\rho > \rho_c$ (see,

e.g., Abbott et al. (The LIGO Scientific Collaboration) (2006, 2008), and references therein; henceforth we adopt $\rho_c = 8$). For this reason, the previous expression for the signal to noise [Eq. (1)] is often re-expressed as

$$\rho = \rho_c w(\theta, \phi, \iota) \frac{D_H(m_1(1+z), m_2(1+z))}{D} \quad (5)$$

which, by comparison with Eq. (1), implicitly defines the *horizon distance* D_H – the maximum luminosity distance to which the detectors are sensitive – as a function of the redshifted masses $m_1(1+z)$ and $m_2(1+z)$ of the binary (see, e.g., Anderson et al. (2001), Finn & Chernoff (1993) and Flanagan & Hughes (1998) for a brief review of the theory underlying the direction-dependent LIGO sensitivity as well as for expressions that approximate $D_H(m_1, m_2)$ for low-mass CBC binaries³).

More commonly used is the *volume-averaged distance* D_v , chosen so the volume of a sphere of radius D_v agrees with the average volume enclosed in a (Euclidean) detection surface:

$$D_v^3 = \frac{1}{4\pi} D_H^3 \int d\Omega \frac{d\psi}{\pi} \frac{d \cos \iota}{2} w^3 \simeq (D_H/2.26)^3 \quad (6)$$

The volume averaged distance is a meaningful measure of sensitivity only when the horizon range is much smaller than the Hubble scale.

A *network* of detectors can coherently add signals from each interferometer to increase the signal-to-noise ρ associated with each signal and by implication its reach. To a first approximation, ignoring small differences in sensitivity due to both their intrinsic differences and their orientations,⁴ the combined SNR all interferometers is higher by roughly $\sqrt{\sum_k L_k^2/L_1^2}$ where L_k is the length of the k th interferometer. For example, this factor is approximately $g_N \simeq \sqrt{1+1+1/4} \simeq \sqrt{2.25}$ for the initial LIGO network, consisting of two 4 km and one 2 km interferometer; see Cutler & Flanagan (1994) for details on realistic multidetector beampatterns. However, in part because a network performs more trials of the same data streams (e.g., for each sky position) and is sensitive to both polarizations simultaneously, for the same false alarm rate the network detection threshold $\rho_{c,net}$ is generally greater than the threshold ρ_c for the individual detectors; see for example Cutler & Flanagan (1994) and Buonanno et al. (2003) for a discussion in the case of gaussian noise. One can therefore speak of a single-interferometer (D_H) and network ($D_H^{(n)} \simeq g_N D_H(\rho_c/\rho_{c,net})$) horizon distance. Unfortunately, only expert analysis of real data can determine the sensitivity of real gravitational-wave

³ A more thorough review of the orbital geometry and waveforms underlying the reach of a single-interferometer search for circularly inspiralling point particles can be found in Brown (2004) and (for the more complex case of spinning binaries) in Apostolatos et al. (1994); Buonanno et al. (2003). Additionally, Koppurapu et al. (2008) discusses of how this orientation-dependent sensitivity influences the present-day LIGO search.

⁴ The small bias ($\simeq 10\%$) introduced by this approximation is much smaller than the characteristic uncertainties discussed later in this paper; see, for example, LIGO site location information in LIGO-T980044-10 (available at <http://admdbsrv.ligo.caltech.edu/dcc/>) and the LAL software documentation (available from <http://www.lsc-group.phys.uwm.edu/daswg/projects/lal.html>).

² Peak sensitivity is attained for a source directly overhead with orbital plane normal to the line of sight.

networks, not the least because noise statistics (and therefore $\rho_{c,net}$) are highly detector- and even search-dependent. To avoid ambiguity and misleading approximations, we henceforth provide results for single, idealized interferometers assuming a detection threshold of $\rho_c = 8$ (e.g., appropriate to gaussian noise). This reference sensitivity agrees with the customary sensitivity measure used in the LIGO coalescence search, a threshold of $\rho_c = 8$ for a single detector as part of a network.⁵ For sources in the local universe, without loss of generality the reader can scale our results to any realistic network and search.

For sources of sufficiently low mass ($M_{tot} \lesssim 20M_\odot$), LIGO is primarily sensitive to less-relativistic and therefore better-understood phases of the spiral-in, allowing us to approximate the waveform by its Newtonian limit (Peters 1964). After considerable algebra (see, e.g. Flanagan & Hughes 1998; Cutler & Flanagan 1994), the signal-to-noise due to an optimally-oriented inspiral at comoving distance r (corresponding to a redshift $z(r)$) can be related to the strain sensitivity S_h by

$$\rho^2 = \frac{5w^2[\mathcal{M}_c(1+z)]^{5/3}}{6\pi^{4/3}D^2} \int_0^\infty df \frac{f^{-7/3}}{S_h(f)} \quad (7)$$

where $\mathcal{M}_c \equiv (m_1 m_2)^{3/5} / (m_1 + m_2)^{1/5}$ is the ‘‘chirp mass’’ of the binary. Based on this expression, individual interferometers in the initial⁶, and advanced⁷ LIGO networks can see *low-mass* binaries out to a horizon (volume-averaged) distance

$$D_{H(v)} \simeq \mathcal{C}_{H(v)} (\mathcal{M}_c / 1.2M_\odot)^{5/6} \quad (8)$$

where $\mathcal{C}_{H(v)} = 31(14)$ Mpc and $\mathcal{C}_{H(v)} = 445(197)$ Mpc respectively. For clarity, the distance \mathcal{C}_v will henceforth be denoted D_{bns} , the volume-averaged distance to which a binary neutron star inspiral can be detected by a single interferometer as part of a network.

In terms of this horizon distance D_H , the intrinsic present-day rate of events per unit comoving volume $\mathcal{R}(0)$, and the chirp mass distribution of merging binaries $p(\mathcal{M}_c)$, the average rate of events with $\rho > \rho_c$ occurring in the nearby universe can be expressed as

$$R_D = \mathcal{R}(0) \int_{\frac{wD_H}{D} > 1} r^2 dr d\Omega \frac{d\psi}{\pi} \frac{d \cos i}{2} p(\mathcal{M}_c) d\mathcal{M}_c \quad (9)$$

$$= \mathcal{R}(0) \left[\int d\mathcal{M}_c \frac{4\pi}{3} D_v(\mathcal{M}_c)^3 p(\mathcal{M}_c) \right]. \quad (10)$$

where the integral is taken over all detectable combinations of masses, orientation, and location. For the lowest-mass binary mergers, for which Eq. (8) applies, the chirp

⁵ For the real LIGO interferometers, no single detector search at this threshold is possible; multi-detector coincidence is required to reduce the nongaussian background to roughly the level indicated (hence ‘‘as part of a network’’).

⁶ We use a published LIGO S5 sensitivity (for the LHO interferometer, on March 13th, 2006), available at http://www.ligo.caltech.edu/~jzweig/distribution/LSC_Data.

⁷ We adopt an advanced LIGO noise curve from LIGO T0900288, available as `ZERO_DET_high_P.txt` at <http://dcc.ligo.org/DocDB/0002/T0900288/002/>. This noise curve is taken from the GWINC program with Mode 1b parameters, as described in LIGO document LIGO-T070247-01-1: 125 W input laser power, 20% signal recycling mirror (SRM) transmissivity, and no detuning of the signal recycling cavity.

mass-weighted average simplifies to

$$R_D \simeq \mathcal{R}(0) \frac{4\pi(\mathcal{C}_v)^3}{3} \int p(\mathcal{M}_c) (\mathcal{M}_c / 1.2M_\odot)^{15/6} d\mathcal{M}_c \quad (11)$$

an expression that has been applied extensively in the literature to translate event rates per unit volume into LIGO detection rates (see, e.g. O’Shaughnessy et al. 2008b, and references therein).

Advanced detectors can see back to an epoch with noticeably different star formation history ($z > 0.1$). Because of each detector’s beampattern, the peak redshift and therefore peak star formation history inside the detection volume varies significantly with sky location. The straightforward generalization of Eq. (9) to arbitrary-redshift sources is presented in the Appendix.

3. MULTICOMPONENT STAR FORMATION HISTORY

The LIGO detection rate depends on the mass distribution of merging binaries $p(\mathcal{M}_c)$ and on the average rate of mergers per unit comoving volume, $\mathcal{R}(t)$. This rate, in turn, generally depends on the net contribution from multiple star-forming populations, a contribution that convolves the star formation rate in each component (the subject of the present section) with the rate at which each component’s star-forming gas yields CBC mergers (the subject of § 4). More specifically, the merger rate density $\mathcal{R}(t)$, a quantity required to calculate the detection rate, is obtained from (i) the star formation rate in each component $d\rho_C/dt$ where C indexes the different star-forming types, $C = e$ for ellipticals and s for spirals, defined as the mass per unit comoving volume and time that forms as stars; (ii) the mass efficiency λ_C at which each type of CBC binaries form, defined as the total number of binaries that survive isolated evolution and form CBC binaries per unit star forming mass; and (iii) the probability distribution dP_{mC}/dt for merger events to occur after a delay time t after star formation, where dP_{mC} is the fraction of mergers occurring between t and $t + dt$ after the progenitor binary forms at $t = 0$:

$$\mathcal{R}(t) = \sum_C \mathcal{R}_C(t) \quad (12)$$

$$\mathcal{R}_C(t) = \int_{-T}^t dt_b \lambda_C \frac{dP_{mC}}{dt}(t - t_b) \frac{d\rho_C}{dt}(t_b) \quad (13)$$

where the integration variable t_b is time at which $\lambda d\rho$ binaries per unit volume are born. As first recognized by de Freitas Pacheco et al. (2006) and as demonstrated systematically in PS-GRB, a multicomponent star formation history that includes both elliptical and spiral galaxies must be applied when calculating present-day merger rates of double compact objects. Simply put, even though elliptical galaxies formed stars long ago, dP/dt decays slowly enough (roughly as $1/t$; see, e.g., PS-GRB) that the high rate of star formation in the early universe can lead to a significant elliptical-galaxy-hosted merger rate density in the present-day universe. Because elliptical galaxies have distinctly different star forming conditions (e.g., metallicities) than present-day star-forming galaxies, models for stellar evolution in the universe should not require identical behavior in present-day solar-metallicity galaxies and in young ellipticals. A

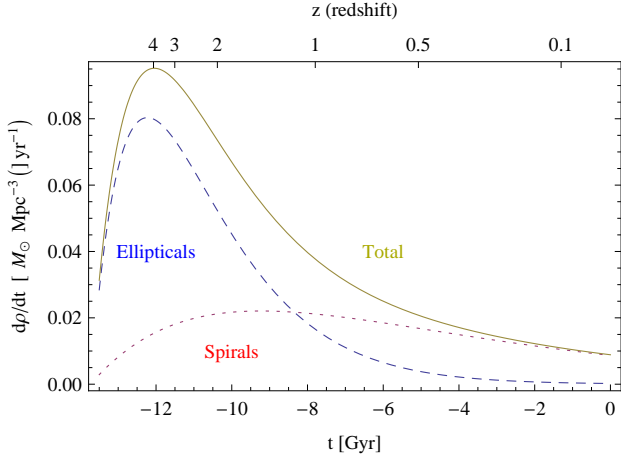


FIG. 1.— Star formation history of the universe used in this paper versus time, relative to the present day. Solid line: Net star formation history implied by Eq. (14). Dashed, dotted line: The star formation history due to elliptical and spiral components.

full multicomponent treatment is necessary. The first multicomponent star formation history was applied to predict BH-NS and NS-NS merger rates in PS-GRB; this paper employs the same framework and preferred star formation history, discussed below.

We adopt the two-component star formation history model presented by Nagamine et al. (2006). This model consists of an early “elliptical” component and a fairly steady “spiral” component, with star formation rates given by

$$\dot{\rho} = \dot{\rho}_e + \dot{\rho}_s \quad (14)$$

$$\dot{\rho}_C = A_C(t/\tau_C)e^{-t/\tau_C} \quad (15)$$

where cosmological time t is measured starting from the beginning of the universe and where the two components decay timescales are $\tau_{e,s} = 1.5$ and 4.5 Gyr, respectively (see Section 2 and Table 2 of Nagamine et al. 2006). These normalization constants $A_{e,s} = 0.22, 0.06 M_\odot \text{yr}^{-1} \text{Mpc}^{-3}$ were chosen by Nagamine et al. (2006) so the integrated amount of elliptical and spiral star formation reproduce the present-day census of baryonic matter in ellipticals and spirals, allowing for a certain fraction of gas recycling between different generations of stars.⁸ Figure 1 illustrates the star formation rates assumed by the model adopted here.

Each component forms stars in its own distinctive conditions, set by comparison with observations of the Milky Way and elliptical galaxies. We assume mass converted into stars in the fairly steady “spiral” component with solar metallicity and with a fixed high-mass IMF power law [$p = -2.7$ in the broken-power-law Kroupa IMF; see Kroupa & Weidner (2003)]. On the other hand, we assume stars born in the “elliptical” component are drawn from a broken power law IMF with high-mass index within $p \in [-2.27, -2.06]$ and metallicity Z within $0.56 < Z/Z_\odot < 1.5$. These elliptical birth conditions agree with observations of both old ellipticals in the local universe (see Li et al. 2006, and references therein) as well as of young starburst clusters (see Fall et al. 2005;

⁸ Our previous paper PS-GRB incorrectly listed a larger value $A_s = 0.15 M_\odot \text{yr}^{-1} \text{Mpc}^{-3}$.

Zhang & Fall 1999, and references therein).

Since two independent stellar populations give birth to CBCs, the net detection rate R_D is the sum of the detection rate due to ellipticals and spirals. In particular, the probability distribution function for R_D is necessarily the convolution of the distribution functions for detection rates due to elliptical and spiral galaxies, respectively. Because of the many orders of magnitude uncertainty in merger rates and the need to smooth across relative errors, however, all our PDFs are stored and smoothed in a logarithmic representation, as $p(\log R_D)$; see for example PS-GRB. For this reason, the convolution takes on an unusual form, involving an integral over the fraction f of the detection rate due to ellipticals (i.e., $f = R_{D,e}/R_D$). Using this variable to form the logarithmic convolution, the distribution for the net rate $\log R_D$ can be calculated from the distributions for ellipticals and spirals ($p_{e,s}$) as

$$p(\log R_D) = \int_0^1 \frac{df}{f(1-f)\ln(10)} \times p_e(\log R_D + \log f) \times p_s(\log R_D + \log(1-f)) \quad (16)$$

$$\equiv p_s \oplus p_e \quad (17)$$

Limitations of two-component model: Our two component model implicitly adopts two extremely strong assumptions: (i) that metallicity in each component does not significantly evolve with redshift and (ii) that all star-forming gas in each component is identical. While sufficient for most problems involving binary evolution, these approximations may be particularly ill-suited to determining the progenitors of gravitational wave detections. Very low metallicity environments could produce BHs with exceptionally high mass; also, the BH binary merger rate increases strongly with metallicity (see, e.g. Belczynski et al. 2009). Because of the long typical delay between progenitor birth and BH-BH merger, very low-metallicity environments in the early universe could contribute significantly to the present-day gravitational-wave detection rate Belczynski et al. (2008a). Even at present, low-metallicity environments exist often enough to potentially dominate the local merger rate (see, e.g., O’Shaughnessy et al. 2008c). For example, the nearby BH-BH progenitor binary IC 10 X-1 both lies in a low metallicity environment and suggests a high BH-BH detection rate for initial LIGO ($O(0.5)$ yr, strongly dependent on survey selection effects; see Bulik et al. (2008)).

Despite strong theoretical and observational evidence for a significant low-metallicity contribution, we have neither the confidence in the necessary astrophysical inputs (i.e., a redshift-dependent metallicity distribution) nor the required database of simulations to include these metallicity effects at this time. Further, unless initial LIGO detects BH-BH mergers, the peak detection rates cannot be significantly larger than what our model family predicts; see Figure 4. For this reason we continue to adopt the simple and conservative two-component mechanism outlined above.

Relation to blue light density: Previously, merger rate estimates for the Milky Way have been scaled up to the local universe, assuming mergers track blue light (see, e.g. Kopparapu et al. 2008, and references therein). As roughly speaking blue light traces star formation

(see, e.g. Kennicutt 1998; O’Shaughnessy et al. 2008c), this extrapolation roughly agrees with our estimate for binary merger rates in spiral-like galaxies, with a suitable choice of normalization (i.e., star formation rate per unit blue light); see the conclusions for a detailed numerical comparison. O’Shaughnessy et al. (2008c) explains why blue light normalization was not adopted in this paper.

4. CBC POPULATION SYNTHESIS MODELS

As outlined in § 2 and § 3 [see particularly Eqs. (9,13)], in order to estimate how often CBC binary mergers could be seen with gravitational-wave detectors we must know several features of the CBC population: (i) how many CBC binaries form from any given star forming mass (characterized by the mass efficiency λ); (ii) how long these CBC binaries last between birth as stars and merger through gravitational wave emission (characterized by dP/dt); and (iii) what masses these merging CBC binaries have (characterized by a probability distribution in chirp mass $p(\mathcal{M}_c)$). In the absence of observations, these properties must be obtained from theoretical models of stellar and binary evolution. We study the formation of compact objects with the *StarTrack* population synthesis code, first developed by Belczynski et al. (2002) and recently significantly extended as described in detail in Belczynski et al. (2008b). Since our understanding of the evolution of single and binary stars is incomplete, this code parameterizes several critical physical processes with a great many parameters (~ 30), many of which influence compact-object formation dramatically. In this specific study, in addition to the IMF and metallicity (which vary depending on whether a binary is born in an elliptical or spiral galaxy), seven parameters strongly influence compact object merger rates: the supernova kick distribution (modeled as the superposition of two independent Maxwellians, using three parameters: one parameter for the probability of drawing from each Maxwellian, and one to characterize the dispersion of each Maxwellian), the stellar wind strength, the common-envelope energy transfer efficiency, the fraction of angular momentum lost to infinity in phases of non-conservative mass transfer, and the relative distribution of masses in the binary. For this reason, following methods largely outlined in our previous work in PS-GRB and PSC2, we perform a broad *parameter study* to ensure all plausible population synthesis models have been explored. We include simulations of two different classes of star-forming conditions: “spiral” conditions, with $Z = Z_\odot$ and a high-mass IMF slope of $p = -2.7$, and “elliptical” conditions, with a much flatter IMF slope $p \simeq -2.3$ and a range of allowed metallicities $0.56 < Z/Z_\odot < 1.5$. Though we have performed thousands of simulations of these two types of conditions in the past (e.g., PS-GRB), to obtain better statistics on rare BH-BH events, we have constructed a new set of archives of $N_S \equiv 282$ and $N_E \equiv 206$ simulations of these two type of conditions, respectively. Within each set, we select parameters randomly according to the distributions described above.

The model database described above is statistically very similar to the database PS-GRB previously used to estimate NS-NS and BH-NS merger rates, with one critical exception: the simulations used here are extensive enough to have a statistically significant number of

merging BH-BH binaries. Merging BH-BH binaries are a small fraction of the total BH-BH population and an exceedingly rare consequence of isolated binary evolution. For example, the number (n) of BH-BH binaries in each of our simulations was always by construction 3000 and could be as high as $\text{few} \times 10^3$ (see Figure 7). On the contrary, the number (m) of *potentially merging* BH-BH binaries whose delay between formation and merger is less than 13.5 Gyr is typically $O(30)$; despite our efforts, three of our simulations produced no merging BH-BH binaries at all (Figure 7). Further, among those few simulated binaries the most massive few can be seen to the greatest distance; thus, only a fraction of these m binaries significantly impact the average chirp mass $\langle \mathcal{M}_c^{15/6} \rangle$ [Eq. (9)] calculated therefore our estimate of the detection rate. Given the small number statistics upon which we build our BH-BH detection rate predictions, we very carefully quantify and propagate uncertainties into our estimated BH-BH (and also BH-NS, NS-NS) detection rates.

4.1. Model uncertainty and recent literature

Our simulations do not explore some known model uncertainties that could significantly increase the predicted merger rate. As noted previously, our star forming conditions involve only near-solar metallicity Bulik et al. (2008); Belczynski et al. (2008a, 2009). Additionally, we assumed that the common-envelope evolution of a Hertzsprung gap donor led to stellar merger, not a compact binary. However, as discussed in Belczynski et al. (2007), the alternative and still plausible option will increase the BH-BH merger rate by $\times 500$. Finally, we assume binaries form through isolated evolution alone, not allowing for any enhancement in young globular proto-clusters; see, e.g., O’Shaughnessy et al. (2007b) and Sadowski et al. (2008). As mentioned previously, because these factors should *increase* the detection rate, our results are the predictions of a conservative model family.

Our simulations also do not self-consistently explore all model uncertainties corresponding that are comparable or smaller than the statistical simulation errors described extensively below. For example, as the *StarTrack* code has evolved over the extended assembly of our archive and this paper, our simulations differ somewhat from other contemporary papers that employ it. Notably, unlike Belczynski et al. (2007), we adopt the full Bondi accretion rate during common-envelope evolution; by trapping more mass in the binary, this generally leads to larger detection rates. Also, the *StarTrack* code does not yet fully explore all uncertainties in single star evolution, such as uncertainties in stellar radii (Fryer et al. 1999) and due to rotational effects (see, e.g., de Mink et al. (2009) Maeder & Meynet (2001) and references therein). While our computationally limited exploration cannot give an idealized, fully-marginalized theoretical prediction, our approach is extremely useful for the reverse problem: how this particular concrete, conservative model family can be tested against future gravitational wave observations.

4.2. Properties of all CBC binaries

Though the calculation was applied only to BH-NS and NS-NS mergers, PS-GRB described how to calculate two of the three essential ingredients needed to calculate the CBC detection rate [Eqs. (9,13)]: (i) the number of CBC merger events per unit mass in progenitors (the mass efficiency $\lambda_{C,\alpha}$); and (ii) the probability that given a CBC progenitor, a merger occurs between t and $t+dt$ since the binary's birth as two stars (the delay time distribution $dP_{c,\alpha}/dt$). For example, as in PS-GRB we estimate the mass efficiency λ for forming a merging binary of type K (=BH-BH, BH-NS, NS-NS) from the number n of binary progenitors of K with

$$\lambda = \frac{n}{N} \frac{f_{cut}}{\langle M \rangle} \quad (18)$$

where N is the total number of binaries simulated, from which the n progenitors of K were drawn; $\langle M \rangle$ is the average mass of all possible binary progenitors; and f_{cut} is a correction factor accounting for the great many very low mass binaries (i.e., with primary mass $m_1 < m_c = 4M_\odot$) not included in our simulations at all. Expressions for both $\langle M \rangle$ and f_{cut} in terms of population synthesis model parameters are provided in Eqs. (1-2) of O'Shaughnessy et al. (2007a). We also estimate the delay time distribution as before, by smoothing (in $\log t$) the n simulated delays t between binary formation and merger; see particularly the Appendix of PS-GRB. Finally, though PS-GRB does not mention masses, we use precisely the same logarithmic smoothing technique to estimate dP/dM_c from a set of binaries; see our Appendix.

The procedures described above lead to very reliable results for NS-NS and BH-NS binaries, because many binaries n and even merging binaries m are present in each simulation. However, most simulations have only a few BH-BH binaries whose delays between birth and merger are less than the age of the universe. With so few merging binaries per simulation, statistical uncertainties would severely limit our ability to determine the physically relevant portion of delay time (dP/dt) and chirp mass ($p(\mathcal{M}_c)d\mathcal{M}_c$) distributions based on those binaries alone. However, since gravitational wave decay depends sensitively on the post-supernova orbital parameters of a newly-born BH-BH binary, the population of *merging* BH-BH binaries should be very similar to a population with marginally wider orbits but often dramatically longer decay timescales. For this reason, in this paper we will improve our statistics for dP/dt and $p(\mathcal{M}_c)$ by including nearly-merging binaries with delay times t between birth and merger less than a cutoff $T = 10^5$ Myr, as justified by our studies in the Appendix.

4.3. Varying the Binary Fraction

In our population synthesis simulations we systematically varied almost all parameters that could significantly impact the present-day merger rate. One parameter left unchanged in past studies, however, was the *binary fraction* f_b , defined as the fraction of stellar systems that are binaries. Without loss of generality, our simulations assume *all* stars form in binaries. The merger rates per unit mass implied by a population with a lower binary fraction f_b can be related to the merger rates we calculate

using

$$\mathcal{R}(t|f_b) = \mathcal{R}(t|f_b = 1) \frac{f_b(1 + \langle q \rangle)}{1 + f_b \langle q \rangle} \quad (19)$$

where $\langle q \rangle = \langle m_2/m_1 \rangle$ is the average mass ratio of our initial stellar population and which is varied between population synthesis models. In particular, because the effect of this parameter trivially influences our rate predictions, we can *analytically* incorporate the influence of any prior assumptions regarding the binary fraction f_b .

The true initial binary fraction of stellar populations is not known; it is believed to be between $f_{b,min} = 15\%$ and $f_{b,max} = 100\%$ (Duquennoy & Mayor 1991). For this paper we will assume f_b could equally likely take on any value in this range. For any given population synthesis model, the binary fraction and mass ratio distribution multiplicatively influence the observed detection rate by a factor

$$X \equiv \frac{f_b(1 + \langle q \rangle)}{1 + f_b \langle q \rangle}. \quad (20)$$

which is distributed between X_{min} and $X = 1$ (at $f_b = 1$) according to

$$p(X)dX = \frac{1 + \langle q \rangle}{[\langle q \rangle(X - 1) - 1]^2} \frac{dX}{1 - f_{b,min}} \quad (21)$$

4.4. Uncertainties and smoothing : Sampling errors

Roughly speaking, the relatively small numbers of merging binary black holes in any simulation ($m \lesssim O(100)$) limit our ability to predict the overall detection rate $\log R_D$ more accurately than $1/\sqrt{m} \ln 10$, because of inaccuracies in reproducing both the mass distribution dP/dM_c and the delay time distribution dP/dt . Additionally, the relatively small number of *simulations* of elliptical and spiral galaxies $N_{E,S} \simeq 300 - 400$ provides little chance of discovering high-rate models that are more rare than roughly $1/N$. To allow for these two errors, we must convolve each individual simulation's merger rate with two gaussian kernels representing these uncertainties:

$$K_{sim} = K_o(\log R_D, 1/\sqrt{m} \ln 10) \quad (22)$$

$$K_{samp} = K_o(\log R_D, 1/\sqrt{N} \ln 10) \quad (23)$$

$$K_o(x, s) = \frac{1}{\sqrt{2\pi s^2}} \exp(-x^2/2s^2) \quad (24)$$

As noted above, a third uncertainty is the binary fraction, which we incorporate with the following kernel:

$$K_b(z, \langle q \rangle) \equiv \frac{10^z \ln 10}{1 - f_{b,min}} \frac{1 + \langle q \rangle}{[\langle q \rangle(10^z - 1) - 1]^2} \quad (25)$$

These terms capture the most significant simulation-related sources of error. We have also explored and included several other potential sources of error, including (i) calibration uncertainty in the detector or mismatch in the waveform model (small, typically $O(10\%)$)⁹; (ii)

⁹ Calibration of the amplitude and phase relationships between different measured frequencies can significantly perturb results. The target calibration amplitude error usually cited is $O(10\%)$; see M. Landry (for the LIGO Scientific Collaboration) (2005) and Adhikari et al. (2003) for a detailed survey.

uncertainty in the overall star formation history (a factor roughly 2) and in the relative proportions of elliptical and spiral galaxies (roughly 10%); and (iii) additional sampling errors introduced by the sensitivity of the chirp mass average to a few high-mass binaries ($O(0.1/\sqrt{n_{ef}/\ln 10})$).

4.5. Model prediction for CBC rate densities

To review, using the **StarTrack** population synthesis code, we have explored a representative sample of stellar evolution produced by elliptical galaxies ($N_E = 206$) and spiral galaxies ($N_S = 282$). From these simulations, using the tools indicated in § 4 we carefully extracted their likely properties (e.g., dP/dt), which in turn we convolved with the star formation history of each of the two major components of the universe (§ 3) to generate a preferred present-day merger rate per unit volume $\mathcal{R}_k(0)$ for each model k , for both elliptical and spiral star-forming conditions.

Though the set of model universe merger rates $R_{(e,s)k}$ encompasses many of the most significant modeling uncertainties, to be more fully comprehensive and to arrive at a smooth PDF we convolve of the “model universe” merger rates $R_{s,p}$ and $R_{e,l}$ for $p = 1, \dots, N_S$ and $l = 1 \dots N_E$ with the uncertainty kernels and binary fraction kernel described previously assuming equal prior likelihood for each model (i.e., $P(E_l) = 1/N_E$ and $P(S_p) = 1/N_S$)

$$\bar{K} = (K_{\text{samp}} * K_{\text{sim}} * K_b) \quad (26)$$

$$p_e(\log R_e) = \sum_{l=1}^{N_E} P(E_l) \bar{K}(\log \frac{R_{e,l}}{R_{e,l}}) \quad (27)$$

$$p_s(\log R_s) = \sum_{p=1}^{N_S} P(S_p) \bar{K}(\log \frac{R_{s,p}}{R_{s,p}}) \quad (28)$$

$$p(\log R) = (p_e \oplus p_s) \quad (29)$$

Figure 2 shows all of the kernels \bar{K} . In Figure 3 the thin ($p(\log R)$) and dashed ($p_e(\log R)$) curves correspond precisely to the output of this procedure.

In the above we assume all simulated population synthesis models are equally plausible *a priori*. However, observations of single and binary pulsars significantly affect our perspective regarding the relative likelihood of different models. NS-NS merger rates derived from the observed sample are in fact typically higher than what most population models predict for the Milky Way. We adopt standard Bayesian methods to determine the posterior probability $P(S_p|C)$ for a given spiral-galaxy model S_p ($p = 1 \dots N_S$)

$$P(S_p|C) \propto P(C|S_p)P(S_p) = P(C|S_p)/N_S \quad (30)$$

given the observational constraint C on the present-day spiral-galaxy contribution to the NS-NS merger rate implied by present-day observations of pulsars. We adopt as a constraint the requirement developed in PS-GRB from existing NS-pulsar observations, that the spiral-galaxy merger rate density of double neutron stars lie between 0.15 and $5.8 \text{ Myr}^{-1} \text{ Mpc}^{-3}$ (90% confidence). The probability $P(C|S_p)$ that the p th spiral-galaxy model predicts a rate consistent with observations of double neutron stars is found simply by integrating the

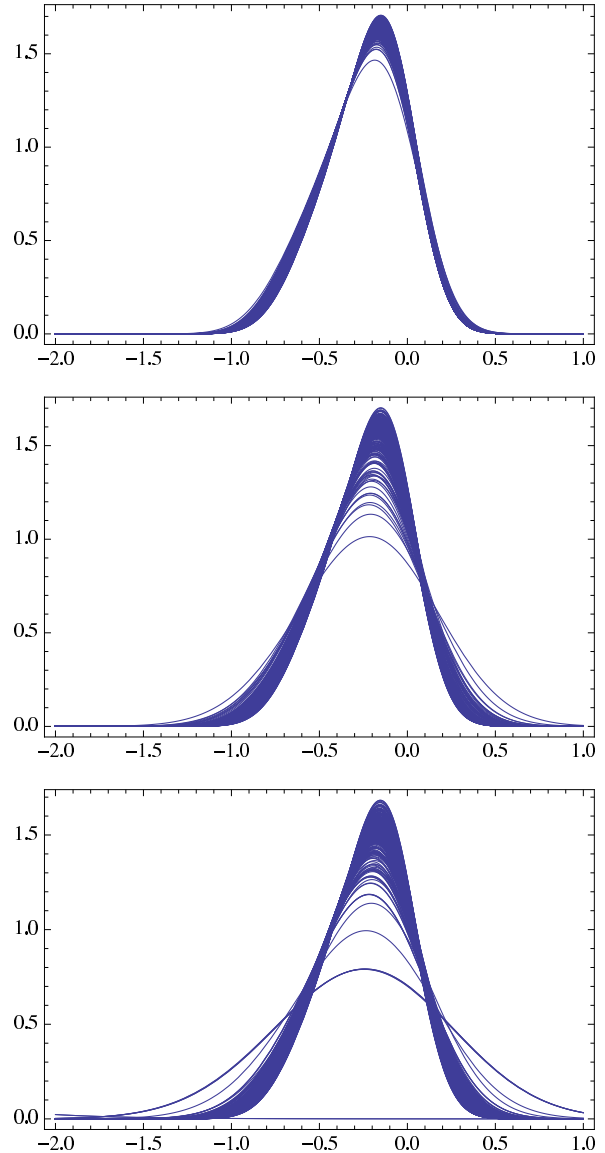


FIG. 2.— All of the kernels \bar{K} versus $\log X$ used in this paper, for NS-NS (top panel), BH-NS (center panel), and BH-BH (bottom panel). As extremely many binaries are available in each simulation, the NS-NS simulations’ uncertainties are dominated by the uncertainty in the binary fraction f_b . Because few BH-BH and occasionally BH-NS binaries are available in each simulation, however, the statistical uncertainty becomes significant.

PDF $P(\log R|S_p)$ for the rate over the constraint interval $C = [0.15, 5.8] \text{ Myr}^{-1} \text{ Mpc}^{-3}$. After renormalizing the probabilities $P(C|S_p)$ into $P(S_p|C)$ by requiring $\sum_p P(S_p|C) = 1$, we arrive at revised predictions for CBC merger rates for BH-BH, BH-NS, and NS-NS binaries as in Eqs. (27-29) but with conditional probabilities:

$$p_s(\log R_s|C) = \sum_{p=1}^{N_S} P(S_p|C) \bar{K}(\log \frac{R_s}{R_{s,p}}) \quad (31)$$

Convolving the constrained spiral rate density distribution p_s with the unconstrained elliptical density p_e leads to our best estimate for the present-day merger rate per unit volume, shown as the thick solid curve in

Figure 3. Our best results favor merger rates between $2 \times 10^{-3} - 0.04 \text{ Mpc}^{-3} \text{ Myr}^{-1}$ for BH-BH mergers (90% confidence), $0.01 - 0.28 \text{ Mpc}^{-3} \text{ Myr}^{-1}$ for BH-NS mergers, and $0.11 - 1.7 \text{ Mpc}^{-3} \text{ Myr}^{-1}$ for NS-NS mergers.

Our previous papers have similarly constrained binary evolution in the Milky Way (PSC2) and in the population of spiral galaxies (PS-GRB). Both interpret observations as much tighter constraints than we do here, because these papers did not allow for error (e.g., in each simulation’s prediction and, for the predictions per unit volume, in the star formation history of the universe). Our bayesian constraints are significantly less restrictive. Our predictions for the posterior NS-NS merger rate are conservative for another, technical reason: we implement the binary fraction as an *uncertainty* rather than a parameter. We therefore cannot rule out very low binary fractions $f_b \simeq 0.1$ in other spiral galaxies, even though a comparison between binary pulsars in the Milky Way and our model database disfavors such low values.

5. CBC DETECTION RATES AND DETECTION PROBABILITY

5.1. CBC Detection Rates for LIGO

Using the **StarTrack** population synthesis code, we have explored a representative sample of stellar evolution produced by elliptical galaxies ($N_E = 206$) and spiral galaxies ($N_S = 282$). From these simulations, using the tools indicated in § 4 we carefully extracted their likely properties (e.g., dP/dt), which in turn we convolved with the star formation history of each of the two major components of the universe (§ 3). Using our understanding of the LIGO range (§ 2) we can convert these merger rate histories into expected single-interferometer LIGO detection rates. Finally, though the set of model universe detection rates $R_{D,(e,s)k}$ encompasses many of the most significant modeling uncertainties, to be more fully comprehensive and to arrive at a smooth PDF we plot in Figure 4 the convolution of the “model universe” detection rates $R_{D,s,p}$ and $R_{D,e,l}$ for $p = 1, \dots, N_p$ and $l = 1 \dots N_E$ with the uncertainty kernels and binary fraction kernel described previously assuming equal prior likelihood for each model (i.e., $P(E_l) = 1/N_E$ and $P(S_p) = 1/N_S$)

$$\bar{K} = (K_{\text{samp}} * K_{\text{sim}} * K_b) \quad (32)$$

$$p_e(\log R_{D,e}) = \sum_{l=1}^{N_E} P(E_l) \bar{K}(\log \frac{R_{D,e}}{R_{D,e,l}}) \quad (33)$$

$$p_s(\log R_{D,s}) = \sum_{p=1}^{N_S} P(S_p) \bar{K}(\log \frac{R_{D,e}}{R_{D,e,p}}) \quad (34)$$

$$p(\log R_D) = (p_e \oplus p_s) \quad (35)$$

and subsequently combine the elliptical and spiral detection rate distributions [Eq. (16)]. [Most of these convolutions can be performed trivially by adding the standard deviations of gaussians in quadrature; the remaining two convolutions are performed numerically.] Though the same basic techniques applied above can be and have been applied to BH-NS and NS-NS binaries previously (PS-GRB), we now incorporate error propagation, a simulation-by-simulation estimate of the relevant chirp mass, and a variable binary fraction; the merger

rate distributions they provide therefore are not proportional to our predictions.

Figure 4 shows the distribution of CBC detection rates predicted by Eq. (10) for individual initial LIGO interferometers as part of a network (thin curves) as well as the contribution from elliptical galaxies alone (dashed curves). As indicated by the close proximity of the elliptical and total merger rate distributions, most BH-BH mergers that LIGO detects should be produced in elliptical galaxies. This elliptical bias arises because BH-BH binaries have long delays between their formation and eventual merger; their present-day merger rate is more easily influenced by ancient star formation. On the other hand, the difference between the dashed and thin curves in the bottom left panel indicate that the NS-NS merger rate must be *spiral*-dominated.

Because the initial LIGO detectors essentially probe different-sized volumes of the local universe for each merger type, their detection rate distributions are identical to those of any similar-scale single- or multiple-IFO network, mod a constant horizontal offset determined by the relative increase in volume NS-NS binaries can be seen [$\log V_{NS-NS}/4\pi(14 \text{ Mpc})^3/3$]. Similarly, because a single advanced LIGO detector’s reach to NS-NS and BH-NS binaries is often not cosmologically significant, weighting over detector and source orientation, our predictions for NS-NS and BH-NS detection rates are identical to those for initial LIGO, mod an offset [= $\log(197/14)^3 = 3.44$]. However, the typical range of a single detector to BH-BH binaries *does* extend past $z \simeq 0.25$, where the star formation rate is noticeably higher and where cosmological volume and redshift factors become significant. But because of the long delay between BH-BH merger and progenitor birth, the BH-BH merger rate $R(t)$ generally increases much more slowly with redshift than the star formation history. As a result, the single-IFO BH-BH detection rate distribution is also comparable to but slightly less than what we expect after scaling up initial-LIGO results to larger range: a detailed calculation suggests a merger detection rate between $3 - 300 \text{ yr}^{-1}$ (90% confidence), in good agreement with the $20 - 500 \text{ yr}^{-1} (D_{\text{bns}}/197 \text{ Mpc})^3$ (90% confidence) expected from cubic rescaling of the initial LIGO result.¹⁰ For networks of advanced detectors, however, cubic scaling breaks down severely; the range is significant enough to require the full cosmological treatment and network-sensitivity-beampattern averaging presented in the Appendix.

5.2. Comparisons with pulsar observations of Galactic NS-NS binaries

Following the previously-discussed procedure to re-evaluate the likelihood of our spiral-galaxy population synthesis models, we arrive at a distribution of initial LIGO detection rates as indicated in Figure 4. Compar-

¹⁰ In our simulations, the black hole-black hole rates generally are *constant* or *decrease* with redshift, due to the long delay between binary birth and merger. Also, the “redshifting factor” $1+z$ in the detection rate integral implies a slightly smaller comoving 4-volume swept out by the detector’s past light cone per unit time at the maximum redshift: $\int dz dV_c/dz/(1+z) \simeq V_c/(1+z)$. Both these factors suggest the BH-BH detection rate at high redshift will be *lower* than a simple cubic extrapolation of the local-universe result.

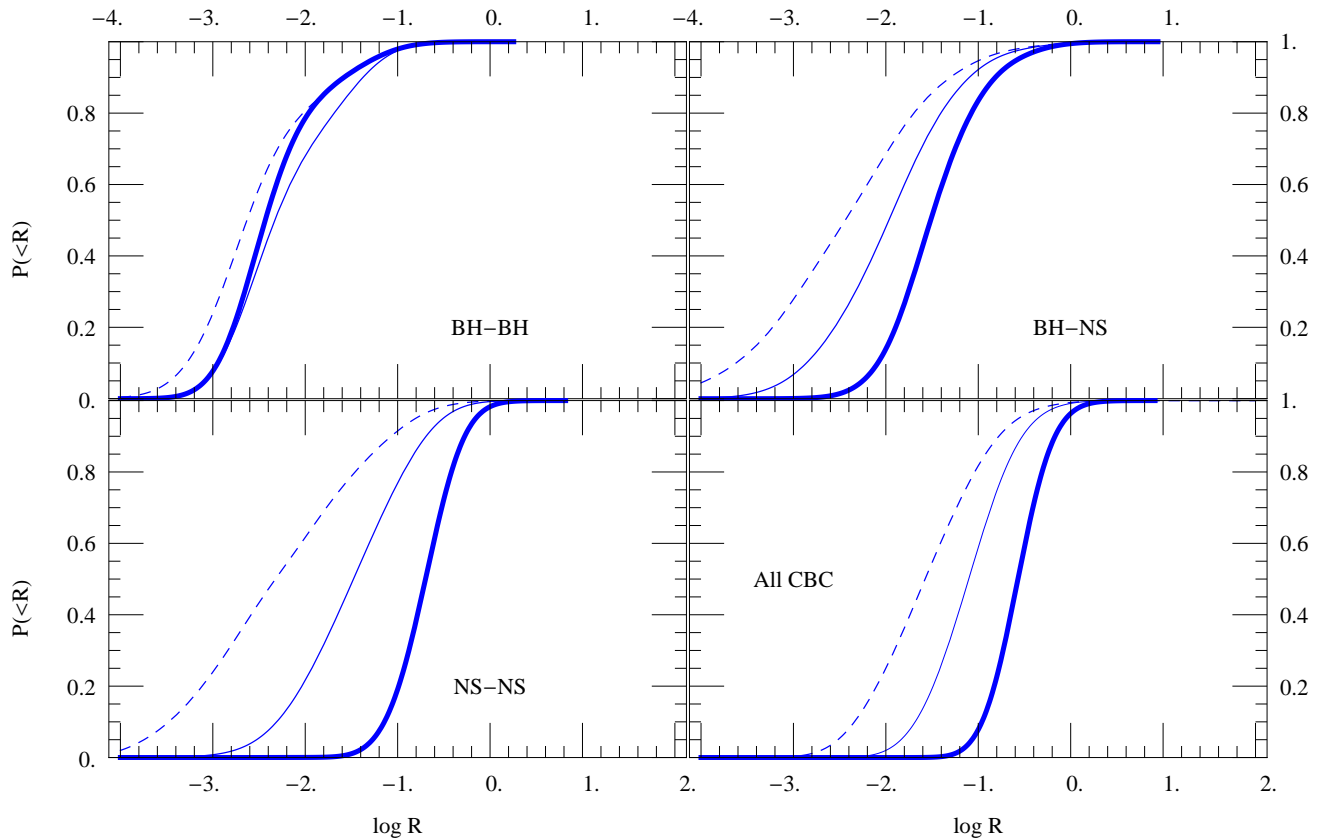


FIG. 3.— Cumulative probability $P(< \log R)$ of various merger rates per unit volume (units $\text{Mpc}^{-3} \text{Myr}^{-1}$), without (thin) and with (thick) requiring consistency with the binary pulsar population in the Milky Way. These distributions incorporate uncertainty in the initial binary fraction, the unknown population synthesis model parameters, and statistical errors implied by the limited size of our simulations. For comparison, the dashed lines show the contribution from *ellipticals only*.

ing these distributions with the unconstrained results of the previous calculation, we arrive at the following conclusions:

Higher NS-NS detection rate: As seen in Figure 3, inferences drawn from the double pulsar population about the present-day NS-NS merger rate lie on the high end of what our models can presently reproduce. By requiring our models reproduce those observations, our constrained distributions naturally favor higher NS-NS detection rates.

Lower BH-BH detection rate from spirals: Compared to our previous results (Fig. 4), the highest binary black hole merger and thus detection rates are ruled out *in spiral galaxies*. Physically, the observational constraint supports those population synthesis models where one particular parameter ($\alpha\lambda$, related to common-envelope evolution) is not exceptionally small ($\alpha\lambda > 0.1$); see for comparison the top left panel of Figure 5 in PSC2. In turn, this parameter $\alpha\lambda$ correlates strongly with the BH-BH merger rate, with low values of $\alpha\lambda$ being required to produce the largest BH-BH merger rates. Thus, because observations of NS-NS binaries in the Milky Way favor high NS-NS merger rates, they disfavor the highest rates of BH-BH mergers in spiral galaxies.

Observations of the NS-NS merger rate in spiral galaxies do not constrain ellipticals, BH-NS well: With the excep-

tion of NS-NS mergers, Figure 4 demonstrates that most *constrained* predictions for LIGO’s detection rate agree strikingly well with our *a priori* expectations. These robust predictions should be expected, since observations of spiral galaxies cannot constrain differences (e.g., due to metallicity and IMF) in the binary evolution in elliptical galaxies. In particular, the single most likely source of a gravitational wave detection in the near future, BH-BH mergers, are due to their long characteristic ages expected to occur primarily in elliptical galaxies; as a result, the present-day BH-BH and total CBC detection rate depends only weakly on our ability to rule out certain population synthesis parameters in spiral galaxies. Furthermore, even in spiral galaxies alone, as seen in PSC2 and references therein, the NS-NS and other CBC merger rates are not tightly correlated. Thus despite the fairly strong and consistent constraints that double pulsar observations imply for *binary evolution parameters*, as described in detail in PSC2, our overall expectations for LIGO’s detection rate remain largely unchanged.

5.3. Net probability of CBC detection

Factoring in poisson statistics for each model, the *net* prior probability P_d that a single LIGO interferometer with a single-IFO range to NS-NS inspiral of D_{bns} oper-

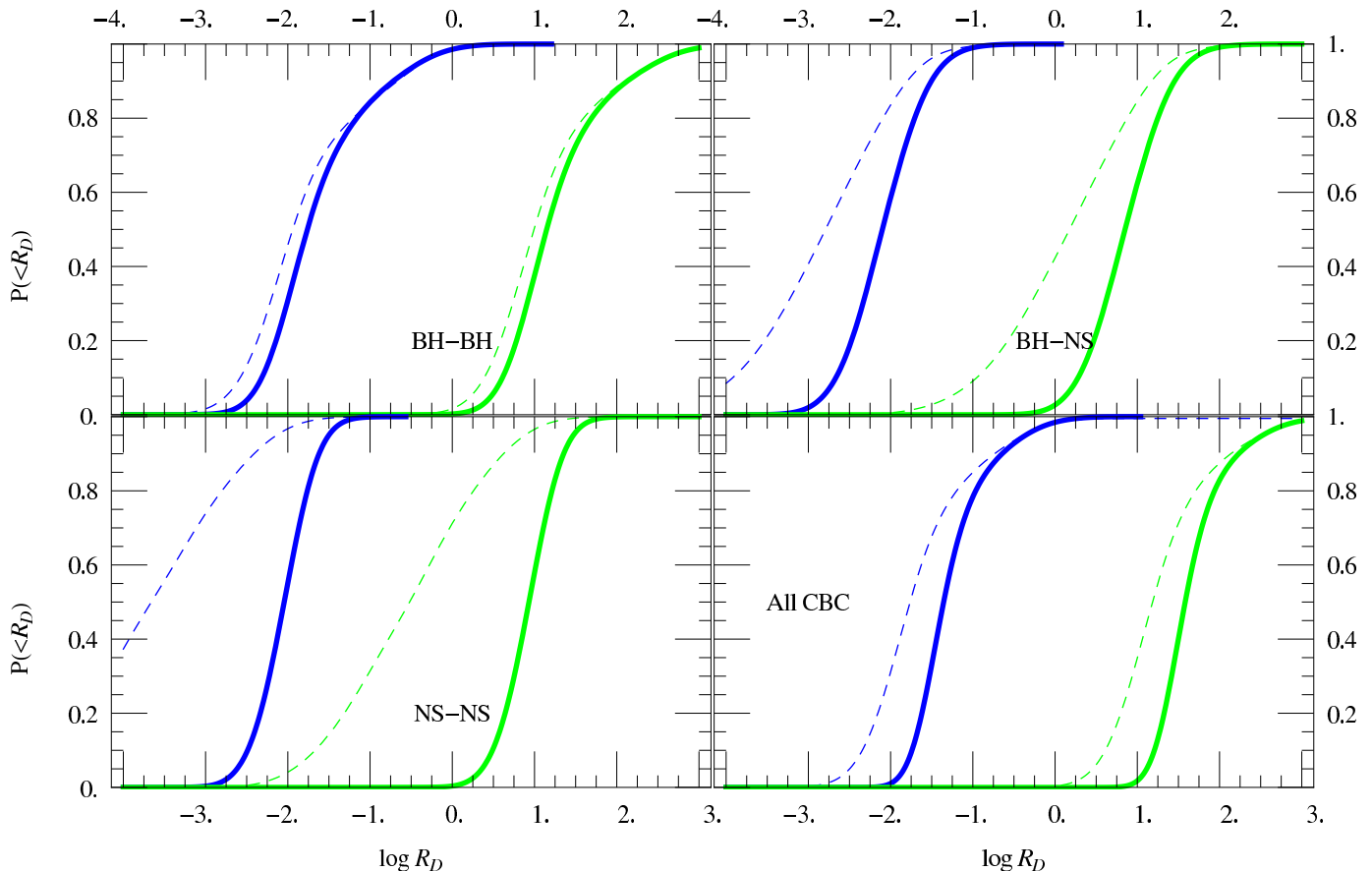


FIG. 4.— Cumulative probability $P(< \log R_D)$ of various event rates for initial (blue; assuming $D_H = 31$ Mpc) and advanced (green; assuming $D_H = 445$ Mpc) single LIGO interferometers as part of a network, requiring consistency with the binary pulsar population in the Milky Way. These distributions incorporate uncertainty in the initial binary fraction, as discussed in the text, as well as uncertainty in the many population synthesis model parameters. For comparison the dashed curves show the contribution from *ellipticals only*.

ating for time T can make at least one detection is

$$P_{\text{detect}}(\geq 1 | D_{\text{bns}}, T) = \int dR_D p(R_D) (1 - e^{-R_D T}) \quad (36)$$

where D_{bns} implicitly enters as a scale factor for R_D ($\propto D_v^3$). More generally, for a multi-interferometer configuration with a time-varying network sensitivity, the appropriate detection probability can be easily calculated from our reference probability by replacing T in the above expression by $\int dt (D_{\text{bns}}(t)/D_{\text{bnsref}})^3$; the latter quantity characterizes the 4-volume to which the search is sensitive. This detection probability can be significantly increased by improvements in the LIGO detector or run schedule that improve the detection 4-volume VT . Assuming a fixed, orientation-averaged range D_{bns} for any fraction of the whole LIGO network, the total probability of detecting one or more events by that fractional network can be approximated by

$$P_{\text{detect}}(\geq 1 | 14 \text{ Mpc}, T) \simeq 0.4 + 0.5 \log(T/8 \text{ yr}) \quad (37a)$$

$$P_{\text{detect}}(\geq 1 | 197 \text{ Mpc}, T) \simeq 0.4 + 0.5 \log(T/0.01 \text{ yr}) \quad (37b)$$

for T between 1 yr and 100 yr or 2×10^{-3} and 0.1 yr, respectively. These approximations are shown in Figure 5.

Equivalently, our calculations suggest that a gravitational-wave network must have a 4-volume sensitivity of $1.3 \times 10^5 \text{ Mpc}^3 \text{ yr}$ (roughly equivalent to a

32 Mpc sphere for 1 year) in order to have a 50% chance of detecting one or more events, as

$$P_{\text{detect}}(\geq 1 | D_{\text{bns}}, 1 \text{ yr}) \simeq 0.5 + 1.5 \log D_{\text{bns}}/32 \text{ Mpc} \quad (38)$$

for D_{bns} between 20 and 70 Mpc.

6. CONCLUSIONS

In this paper, we provide the first estimate of the CBC detection rate for initial and advanced LIGO which accounts for (i) star formation in both elliptical and spiral galaxies as a function of redshift, (ii) binary black holes, (iii) a range of plausible binary fractions, and most significantly (iv) a large range of plausible binary evolution scenarios. Our results strongly indicate that that existing gravitational wave detectors are at the threshold of detection; that moderate improvements in these detectors, such as the enhanced LIGO upgrade of 2009, could plausibly lead to detecting at least one binary merger in a year of operation; that advanced LIGO detectors should be reasonably expected to detect inspirals over 1-2 yr of operation; and that even the absence of a detection by advanced interferometers would very significantly constrain the set of model parameters that could be consistent with observations.

Our predicted detection rates are somewhat higher than those presented in PSC2 because we include elliptical galaxies: mergers in elliptical galaxies dominate our estimates of the BH-BH and BH-NS event

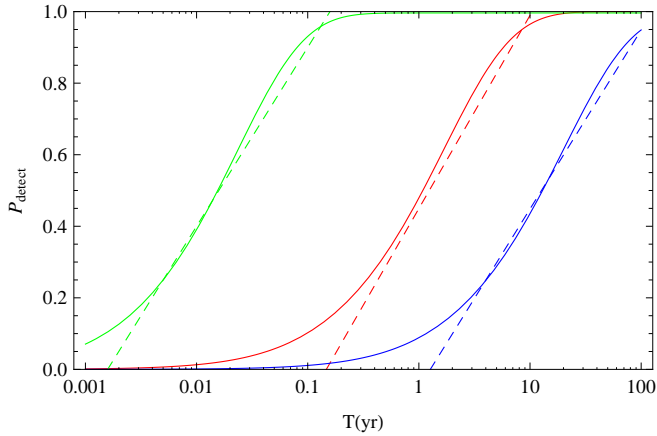


FIG. 5.— Probability $P_{\text{detect}}(\geq 1|D_{\text{bns}}, T)$ [Eq. (36)] of detecting at least one CBC merger in time T yr by a single interferometer as part of a network with volume-averaged range $D_{\text{bns}} = 14$ Mpc (solid blue), 32 Mpc (solid red) and 197 Mpc (solid green) to double-neutron star inspiral, taking into account information about binary pulsars in the Milky Way. For comparison, the dashed curves corresponds to the approximations presented in Eq. 37.

rates. However, our previous estimates effectively assumed a high present-day star formation rate per unit volume: an assumed Milky Way-equivalent galaxy density of $0.01/\text{Mpc}^3$ and star formation rate per spiral galaxy of $3.5M_{\odot}/\text{yr}$ correspond to a present-day star formation rate three times higher than observed. For this reason, a naive product of the merger rates per Milky Way galaxy drawn from PSC2’s Figure 6 leads to preferred merger rates per unit volume that agree well our preferred values. For example, our current results and this naive rescaling of PSC2 results both favor local merger rate densities of $10^{-2}\text{Mpc}^{-3}\text{Myr}^{-1}$ for black hole-neutron star binaries and $3 \times 10^{-2}\text{Mpc}^{-3}\text{Myr}^{-1}$ for binary neutron stars. Correcting for the star formation history normalization, however, our calculations suggest three times as many mergers per volume for BH-NS and NS-NS than in PSC2. Similarly, our predicted detection rates are higher than those implied by Figure 7 in PSC2, correcting for the previously mentioned star formation rate bias (reducing the rates shown in that figure by 3) and rescaling to a single-interferometer rather than network range (reducing the rate by $\times 10$).

Limiting attention to elliptical- plus spiral-galaxy models that include only those spiral galaxy history models that reproduce current observations of double pulsars, we find that a single detector in the initial LIGO network should be sensitive to 2.4×10^{-2} – 0.46 $(\rho_c/8)^{-3}(D_{\text{bns}}/14\text{Mpc})^3$ mergers per year (90% confidence level), where we sum over all merger types to produce an overall detection rate, where $\rho_c = 8$ is the threshold SNR of the search and D_{bns} is the radius of the effective volume inside of which a single detector in the appropriate array could observe the inspiral of two $1.4M_{\odot}$ neutron stars. We estimate that the LIGO detector network has a probability $P_{\text{detect}}(\geq 1) \geq 0.4 + 0.5 \log(V/V_c)(T/8\text{yr})$ of detecting a merger during each year of operation, where $V = 4\pi D_{\text{bns}}^3/3$ is the volume to which a multidetector search for binary neutron star inspiral is sensitive, V_c is the volume inside a

14 Mpc radius sphere, and $1/3 < (V/V_c)(T/\text{yr}) < 8$. For example, the probability P_{detect} of detecting one or more mergers can be approximated by (i) $P_{\text{detect}} \simeq 0.4 + 0.5 \log(T/0.01\text{yr})$, assuming $D_{\text{bns}} = 197\text{Mpc}$ and it operates for T years, for T between 2 days and 0.1 yr); or by (ii) $P_{\text{detect}} \simeq 0.5 + 1.5 \log D_{\text{bns}}/32\text{Mpc}$, for one year of operation and for D_{bns} between 20 and 70 Mpc.

In this paper we have continued to employ approximate waveform and detection models to estimate the sensitivity of ground-based gravitational wave detectors to moderate-mass ($M \simeq 10M_{\odot}$) BH-BH mergers (see, e.g., Flanagan & Hughes (1998) and Buonanno et al. (2003) for a review). Advanced detectors, however, will be sensitive at cosmological distances to the later phases of high-mass mergers, a complex strong-field and strongly-precessing regime which is only beginning to be thoroughly understood through numerical simulations. Progress in numerical waveform modeling and search pipeline analysis is required to better understand how often these candidates could be identified, especially for spinning systems, as expected in nature.

The authors appreciate helpful comments received from Ilya Mandel, Alberto Vecchio, Patrick Brady, Chad Hanna, Steve Fairhurst, Tania Regimbau, Alan Weinstein, and all the members of LIGO inspiral search group. **Grants** R.O. was supported by National Science Foundation awards PHY 06 -53462 and the Center for Gravitational Wave Physics. The Center for Gravitational

Wave Physics is supported by the George A. and Margaret M. Downsborough Endowment and by the National Science Foundation under cooperative agreement PHY 01-14375. VK was supported by NSF grant PHY-0653321. KB acknowledges the support from the Polish Ministry of Science and Higher Education (MSHE) grant N N203 302835 (2008-2011).

REFERENCES

- Abbott et al. (The LIGO Scientific Collaboration). 2003, (gr-qc/0308043) [URL]
 —. 2006, *Phys. Rev. D*, 73, 062001 [ADS]
 —. 2008, *Phys. Rev. D*, 77, 062002 [URL]
- Abbott et al. (The LIGO Scientific Collaboration), B. 2009, (arXiv:0901.0302) [URL]
- Acernese, F., Amico, P., Alshourbagy, M., Antonucci, F., Aoudia, S., Avino, S., Babusci, D., Ballardin, G., Barone, F., Barsotti, L., Barsuglia, M., Beauville, F., Bigotta, S., Birindelli, S., Bizouard, M. A., Boccara, C., Bondu, F., Bosi, L., Bradaschia, C., Braccini, S., Brilliet, A., Brisson, V., Brocco, L., Buskulic, D., Calloni, E., Campagna, E., Cavalier, F., Cavalieri, R., Cella, G., Cesarini, E., Chassande-Mottin, E., Corda, C., Cottone, F., Clapson, A.-C., Cleva, F., Coulon, J.-P., Cuoco, E., Dari, A., Dattilo, V., Davier, M., DeRosa, R., Di Fiore, L., Di Virgilio, A., Dujardin, B., Eleuteri, A., Enard, D., Ferrante, I., Fidecaro, F., Fiori, I., Flaminio, R., Fournier, J.-D., Francois, O., Frasca, S., Frasconi, F., Freise, A., Gammaitoni, L., Garufi, F., Gennai, A., Giazotto, A., Giordano, G., Giordano, L., Gouaty, R., Grosjean, D., Guidi, G., Hebri, S., Heitmann, H., Hello, P., Holloway, L., Karkar, S., Kreckelbergh, S., La Penna, P., Laval, M., Leroy, N., Letendre, N., Lorenzini, M., Lorette, V., Loupias, M., Losurdo, G., Mackowski, J.-M., Majorana, E., Man, C. N., Mantovani, M., Marchesoni, F., Marion, F., Marque, J., Martelli, F., Masserot, A., Mazzoni, M., Milano, L., Moins, C., Moreau, J., Morgado, N., Mours, B., Pai, A., Palomba, C., Paoletti, F., Pardi, S., Pasqualetti, A., Passaquieti, R., Passuello, D., Perniola, B., Piergiovanni, F., Pinard, L., Poggiani, R., Punturo, M., Puppo, P., Qipiani, K., Rapagnani, P., Reita, V., Remillieux, A., Ricci, F., Ricciardi, I., Ruggi, P., Russo, G., Solimeno, S., Spallicci, A., Stanga, R., Taddei, R., Tonelli, M., Toncelli, A., Tournefier, E., Travasso, F., Vajente, G., Verkindt, D., Vetrano, F., Viceré, A., Vinet, J.-Y., Vocca, H., Yvert, M., & Zhang, Z. 2006, *Classical and Quantum Gravity*, 23, 635 [ADS]
- Adhikari, R., González, G., Landry, M., O'Reilly, B., & the LIGO Scientific Collaboration. 2003, *Classical and Quantum Gravity*, 20, 903 [ADS]
- Anderson, W. G., Whelan, J. T., Brady, P. R., Creighton, J. D. E., Chin, D., & Riles, K. 2001, *Beam Pattern Response Functions and Times of Arrival for Earthbound Interferometers*, *Tech. Rep. LIGO-T010110-00-Z*, LIGO Project [URL]
- Apostolatos, T. A., Cutler, C., Sussman, G. J., & Thorne, K. S. 1994, *Phys. Rev. D*, 49, 6274 [ADS]
- Belczynski, K., Bulik, T., Fryer, C. L., Ruiter, A., Vink, J. S., & Hurley, J. R. 2009, *ArXiv e-prints* [ADS]
- Belczynski, K., Hartmann, D. H., Fryer, C. L., Holz, D. E., & O'Shea, B. 2008a, *ArXiv e-prints* [ADS]
- Belczynski, K., Kalogera, V., & Bulik, T. 2002, *ApJ*, 572, 407 [ADS]
- Belczynski, K., Kalogera, V., Rasio, F., Taam, R., Zezas, A., Maccarone, T., & Ivanova, N. 2008b, *ApJS*, 174, 223 [URL] [ADS]
- Belczynski, K., Taam, R. E., Kalogera, V., Rasio, F. A., & Bulik, T. 2007, *ApJ*, 662, 504+ [ADS]
- Brown, D. 2004, *PhD. Thesis*, U. Wisconsin at Milwaukee [URL]
- Brown, G. E. & Bethe, H. A. 1994, *ApJ*, 423, 659 [ADS]
- Bulik, T., Belczynski, K., & Prestwich, A. 2008, (arXiv:0803.3516) [URL]
- Bulik, T., Gondek-Rosinska, D., & Belczynski, K. 2004, *MNRAS*, 352, 1372 [ADS]
- Buonanno, A., Chen, Y., & Vallisneri, M. 2003, 67, 104025 [URL]
- Buonanno, A., Chen, Y., & Vallisneri, M. 2003, *Phys. Rev. D*, 67, 104025 [ADS]
- Cutler, C. & Flanagan, E. 1994, *Phys. Rev. D*, 49, 2658 [ADS]
- de Freitas Pacheco, J. A., Regimbau, T., Vincent, S., & Spallicci, A. 2006, *International Journal of Modern Physics D*, 15, 235 [ADS] [ADS]
- de Mink, S. E., Cantiello, M., Langer, N., Pols, O. R., Brott, I., & Yoon, S.-C. 2009, *A&A*, 497, 243 [ADS]
- Duquenooy, A. & Mayor, M. 1991, *A&A*, 248, 485 [ADS]
- Fall, S. M., Chandar, R., & Whitmore, B. C. 2005, *ApJ*, 631, L133 [ADS]
- Finn, L. S. & Chernoff, D. F. 1993, *Phys. Rev. D*, 47, 2198 [ADS]
- Flanagan, É. É. & Hughes, S. A. 1998, *Phys. Rev. D*, 57, 4535 [ADS]
- Fryer, C., Burrows, A., & Benz, W. 1998, *ApJ*, 496, 333 [ADS]
- Fryer, C. L., Woosley, S. E., & Hartmann, D. H. 1999, *ApJ*, 526, 152 [ADS]
- Kennicutt, Robert C., J. 1998, *Annual Review of Astronomy and Astrophysics*, 36, 189 [URL]
- Kopparapu, R. K., Hanna, C. R., Kalogera, V., O'Shaughnessy, R., Gonzalez, G., Brady, P. R., & Fairhurst, S. 2008, (arXiv:0706.1283) [URL]
- Kroupa, P. & Weidner, C. 2003, *ApJ*, 598, 1076 [URL]
- Kulczycki, K., Bulik, T., Belczynski, K., & Rudak, B. 2006, *A&A*, 459, 1001 [ADS]
- Li, Z., Zhang, F., & Han, Z. 2006, accepted for publication to *ChJAA* (astro-ph/0605610) [URL]
- M. Landry (for the LIGO Scientific Collaboration). 2005, *Classical and Quantum Gravity*, 22, S985 [URL]
- Maeder, A. & Meynet, G. 2001, *A&A*, 373, 555 [ADS]
- Nagamine, K., Ostriker, J. P., Fukugita, M., & Cen, R. 2006, *ApJ*, 653, 881 [URL] [ADS]
- O'Shaughnessy, R., Kalogera, V., & Belczynski, C. 2008a, *ApJ*, 675, 566+ [URL]
- O'Shaughnessy, R., Kalogera, V., & Belczynski, K. 2007a, *ApJ*, 667, 1048 [URL]
- O'Shaughnessy, R., Kim, C., Fragos, T., Kalogera, V., & Belczynski, K. 2005, *ApJ*, 633, 1076 [ADS] [ADS]
- O'Shaughnessy, R., Kim, C., Kalogera, V., & Belczynski, K. 2008b, *ApJ*, 672, 479 [URL]
- O'Shaughnessy, R., Kopparapu, R., & Belczynski, K. 2008c, submitted to *ApJ*; arXiv:0812.0591 [URL]
- O'Shaughnessy, R., O'Leary, R., & Rasio, F. A. 2007b, *Phys. Rev. D*, 76, 061504 [URL]
- Peters, P. 1964, *Physical Review*, 136, 1224 [ADS]
- Portegies Zwart, S. F. & Yungelson, L. R. 1998, *A&A*, 332, 173 [ADS]
- Sadowski, A., Belczynski, K., Bulik, T., Ivanova, N., Rasio, F. A., & O'Shaughnessy, R. 2008, *ApJ*, 676, 1162 [ADS]
- The VIRGO project website. ??? [URL]
- Voss, R. & Tauris, T. M. 2003, *Monthly Notices of the Royal Astronomical Society*, 342, 1169 [URL]
- Zhang, Q. & Fall, S. M. 1999, *Astrophysical Journal*, 527, L81 [URL]

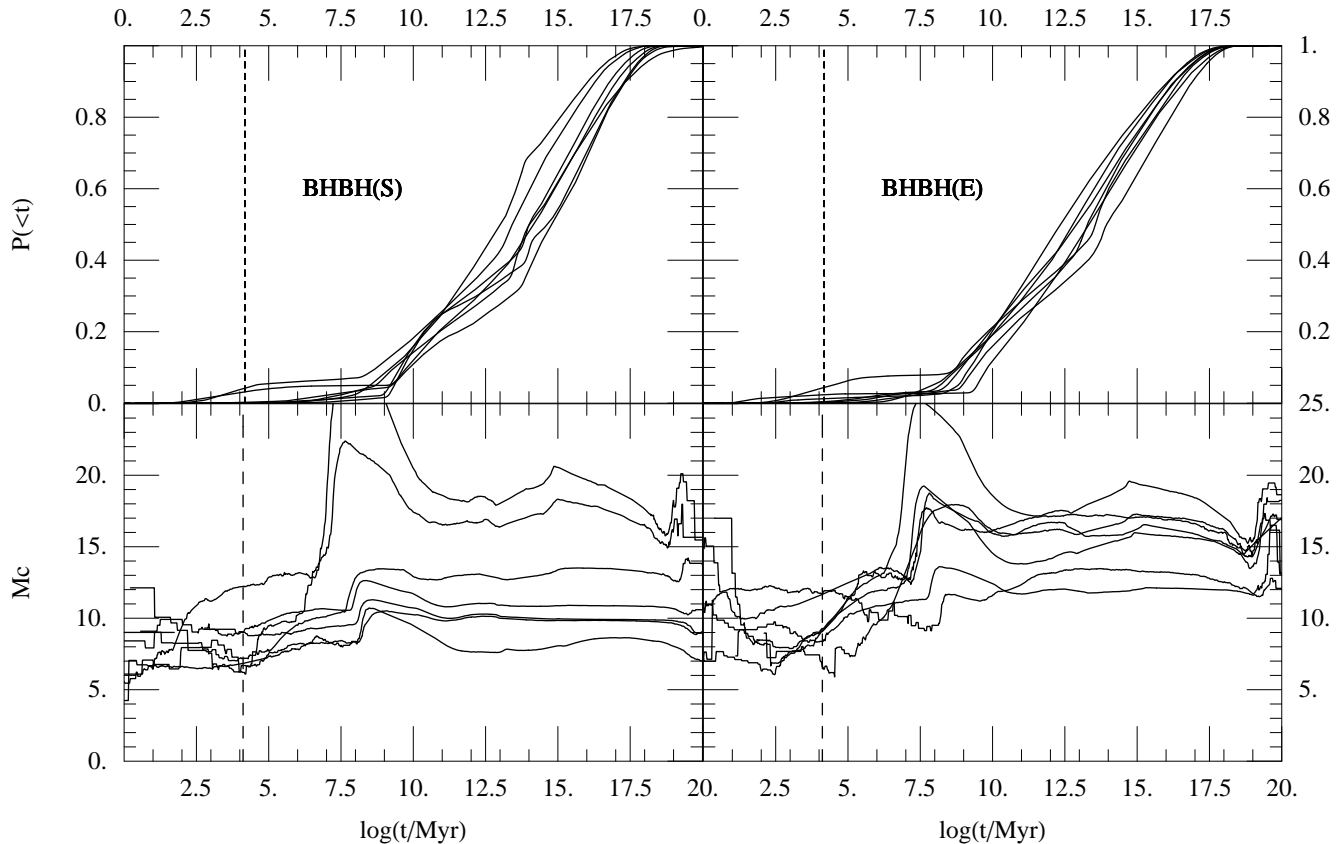


FIG. 6.— Top panels: Cumulative probabilities $P_m(<t)$ that a BH-BH binary will merge in time less than t , for **ten** randomly-chosen population synthesis models that satisfy the limitations discussed in the text, given spiral (left) and elliptical (right) star forming conditions. A vertical dashed line indicates the age of the universe. Given the enormous sample sizes involved – by construction, each sample has at least 3000 binaries – these distributions are expected accurate to within **0.03** almost everywhere (with 90% probability), barring the fine details near the short-time and long-time limits. Bottom panels: Average chirp mass $\bar{M}_c(t)$ [Eq. (A1)] of binaries merging between $0.1t$ and $10t$, versus time. Usually, the binaries that merge within 100 Gyr after their birth have a chirp mass lower than $10M_\odot$, significantly lower than the average chirp mass of more separated holes.

APPENDIX

RECONSTRUCTING THE MASS AND TIME DISTRIBUTIONS

Selecting binaries for mass estimation: We prefer to smooth dP/dt over a shorter timescale than the maximum allowed by evolution of isolated BH-BH binaries. On physical grounds, double BH binaries whose delay times are comparable to or smaller than the age of the universe are more likely to be similar to merging BH-BH binaries (the focus of our study) than wide binaries that have never interacted. To quantify the point at which the transition occurs and therefore the timescale inside of which BH-BH binaries are comparatively similar, we calculate the “average” chirp mass of binaries $\bar{M}_c(t)$ merging within a factor 10 of time t :

$$\bar{M}_c(t) = \left[\frac{\sum_{j:0.1t < t_j < 10t} \mathcal{M}_{c_j}^{15/6}}{\sum_{j:0.1 < t_j < 10} 1} \right]^{6/15} \quad (\text{A1})$$

Figure 6 shows the results of this calculation. Based on the delay time distribution $P_m(<t)$ and average chirp mass of similar binaries $\bar{M}_c(t)$, a sharp distinction exists between binaries with $t \lesssim 10^7$ Myr and wider binaries. These massive wide binaries have orbits largely unaffected by binary evolution and have a delay time distribution $dP/dt \propto 1/t$ largely determined by their initial orbital configuration. On the contrary, tighter and less massive binaries have been significantly perturbed by binary evolution. Within each simulation, they appear to be drawn from a similar chirp mass distribution (allowing for significant sampling-induced fluctuations in $\bar{M}_c(t)$)

Predictions and smoothing: Physical timescales From the above similarity argument, we suspect the n_{eff} BH-BH binaries with delay times $t < 10^5$ Myr are similar to the set of binaries with delay times < 13.5 Gyr. However, even with those binaries we often have only $O(50)$ with which to estimate $p(\mathcal{M}_c)$; the chirp mass distribution must be estimated with smoothing. We use the same approach as is used for dP/dt in PS-GRB to estimate the chirp mass

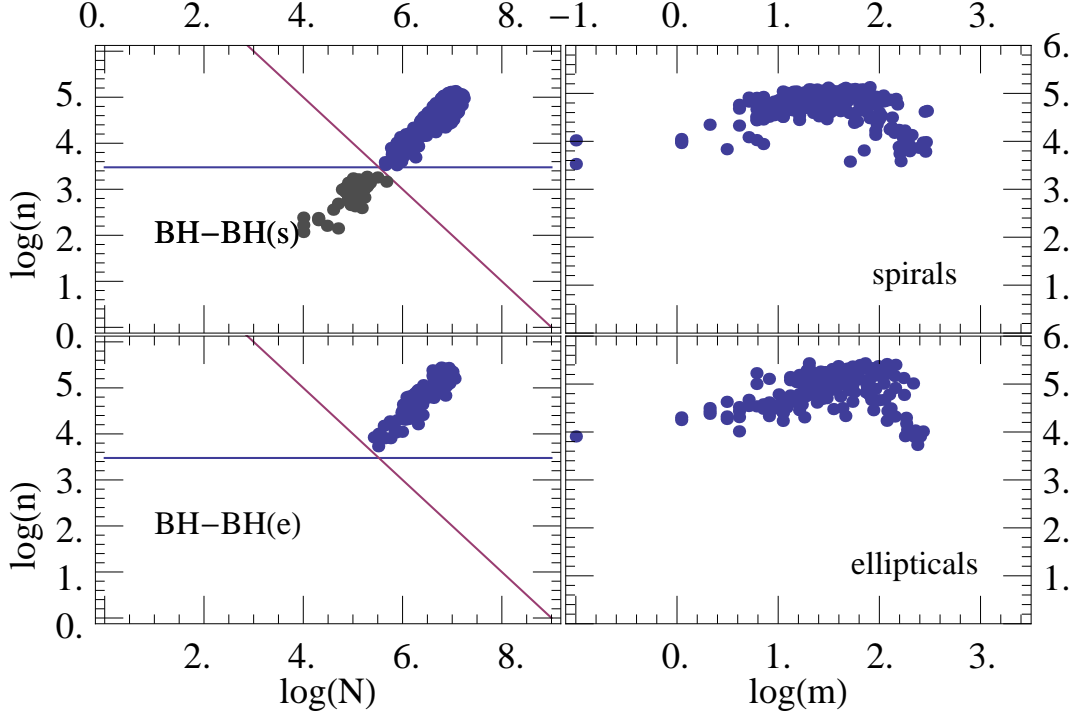


FIG. 7.— Left plot: For spiral (top panels) and elliptical (bottom) archives, a scatter plot of the number of BH-BH binaries n seen in a simulation of N progenitor binaries (each progenitor component having mass greater than $4M_{\odot}$; higher primary masses are drawn from the broken-Kroupa IMF). The two solid lines show the cutoffs $n > 3000$ and $nN > 1 \times 10^9$ imposed to insure data quality and reduce sampling bias. Simulations used in this paper, shown in blue, must lie above and to the right of these cutoffs. Right plot: For the simulations above and to the right of the lines shown to left, scatter plot of the total number of bound BH-BH binaries remaining in the simulation (n) versus the number m of *potentially-merging binaries* (i.e., with a delay between birth and merger less than 13.5 Gyr). Simulations with no mergers ($m = 0$) are shown artificially with $m = 0.1$ so that they can be included in this figure to better indicate how often this occurs in our simulation set.

distribution:

$$\hat{p}(\mathcal{M}_c) \equiv \frac{1}{\mathcal{M}_c n_{eff} \ln 10} \sum_{k=1}^{n_{eff}} \frac{1}{\sqrt{2\pi(s_2)^2}} e^{-(\log \mathcal{M}_c - l_{m,k})^2 / 2(s_2)^2} \quad (\text{A2})$$

$$s_2 \equiv \frac{[(\max_k l_{m,k}) - (\min_k l_{m,k})]}{1.25 \sqrt{n_{eff}}} \quad (\text{A3})$$

where the $l_{m,k} = \log_{10}(\mathcal{M}_c/M_{\odot})$ for $k = 1 \dots n_{eff}$ are the logarithms of each binaries' chirp mass for the n_{eff} binaries with delay times $< 10^5$ Myr.

SAMPLING LIMITATIONS AND ARCHIVE SELECTION

Both sets of simulations are highly heterogeneous: the number of binaries simulated (N), the number of bound BH-BH binaries remaining at the end of stellar evolution (n), and the number of those binaries which merge within 13.5 Gyr (m) all span several orders of magnitude, as shown in Figure 7. Evidently, only for those simulations with *many* BH-BH binaries ($n \gg 1000$) – particularly with several *merging* binaries ($m \gg 1$) – can we reliably extract relevant physics, such as the present-day merger rate and characteristic chirp mass of BH-BH binaries due to a starburst in the early universe. However, as discussed in PS-GRB, the obvious subsets of simulations for which we can reliably make predictions, such as the set of simulations with $n > 3000$, could have been biased, over-representing those simulations which predict more mergers per simulated binary. To mitigate the influence of this bias, in *addition* to requiring that each simulation have many BH-BH binaries ($n > 3000$), we also (or, equivalently, instead) require that $nN > 1 \times 10^9$. The second cut's prefactor (1×10^9) is chosen so that every simulation that satisfies it has $n > 3000$. The subset of simulations which satisfies both conditions has a relatively unbiased distribution of n/N , the fraction of simulated binaries that end up as bound BH-BH binaries (PS-GRB). These two cuts do not introduce biases in any of the parameters: the set of simulations which satisfy these cuts has similar statistical properties as the entire archive

(we omit the many plots needed as proof).

Handling undersampled cases: Finally, with each simulation guaranteed to have 3000 binaries, most simulations have a minimum of $O(1)$ merging BH-BH binaries; see Figure 7 for details. Some simulations still do contain very few binaries that are merging or even nearly so, largely because certain combinations of physical circumstances rarely lead to the formation of many tight black hole binaries. Given that we construct model universes from independent elliptical and spiral simulations, these simulations will lead to an indeterminate, small detection rate in only roughly $1/N_E N_S \simeq O(1/300^2)$ universe models. Even considering only elliptical or spiral galaxy star formation, they influence our predictions roughly $O(1/N_{E,S}) \simeq 1\%$ of the time. We therefore adopt a few percent as the lowest resolvable probability of any event our simulations can resolve. For clarity, in the text we omit these simulations and the implied systematic error bars on our estimates of posterior probabilities. Since they never influence our predictions; we ignore them.

Potential biases in multiply-selected simulations: Just as the set of simulations was reduced to find simulations with many BH-BH binaries in § 4, here we require our simulations *additionally* have enough NS-NS binaries to enable accurate estimates.¹¹ Most population synthesis simulations we performed that produce an adequate number of BH-BH binaries also produce more than enough NS-NS and NS-BH binaries ($\sim 10^4$) to allow us to estimate the three properties ($\lambda, dP/dt, p(\mathcal{M}_c)$) needed to reconstruct merger and detection rates for these NS binaries. However, certain combinations of population synthesis parameters strongly favor merging BH-BH production over NS-NS production. Most of our simulations of these conditions did not produce enough NS-NS binaries to allow accurate estimates. In other words, the set of simulations that have *both* enough NS-NS and close BH-BH binaries is slightly biased against the highest BH-BH and lowest NS-NS merger rates.

The goal of this paper is to determine the relative likelihood of CBC merger and detection rates given existing observations. In particular, in § 5.2 we examine the distribution of BH-BH merger rates for (spiral-galaxy) simulations for which the NS-NS merger rates are consistent with milky Way observations. This subset of simulations is inevitably contained within the biased set of simulations for which NS-NS and BH-BH merger rates can be accurately estimated. That being said, the observational constraints reviewed in § 5.2 point to a high NS-NS merger rate and will therefore inevitably rule out the few models for which NS-NS merger rates could not be accurately determined.

RATES FOR ADVANCED DETECTORS

Networks of advanced ground-based interferometers can detect optimally oriented binaries of moderate-mass black holes (e.g., $M \simeq 10 - 15M_\odot$) at cosmologically significant distances $z \geq 1$. Merger rates on the past light cone of a detector become inhomogeneous (versus redshift) at this scale, simply because the star formation rate increases dramatically near $z \simeq 1 - 2$ during the epoch of galaxy assembly. Under these circumstances, the assumptions used in the traditional approach described in the text breaks down. The detection rate must be integrated over the mass distribution, the full networked orientation-dependent sensitivity, and redshift-dependent merger rate.

For the purposes of this paper, we continue to assume the maximum luminosity distance to which a single interferometer can identify a merger in noise is well-described by the inspiral phase [Eq. 7]. To normalize our estimate, we adopt a single-interferometer advanced LIGO range of 445 Mpc. Based on the optimal range for a given chirp mass, each simulation's the chirp mass distributions, and the single-interferometer beampattern w [Eq. 2], we determine the fraction of all mergers at redshift z that could be detected, $P_{ok}(z)$:

$$P_{ok}(z) = \int_{D(z) < w D_H} \frac{d\Omega}{4\pi} \frac{d\psi}{\pi} \frac{d \cos i}{2} d\mathcal{M}_c p(\mathcal{M}_c) \quad (\text{C1})$$

The overall single-interferometer detection rate is therefore the sum over the past light cone of the (redshifted) rate of mergers on it, times the fraction P_{ok} of mergers that could be detected:

$$R_D = \int dz \frac{dV}{dz} \frac{\mathcal{R}(t)}{1+z} P_{ok}(z) \quad (\text{C2})$$

¹¹ We adopt the same conditions on n and N as were used in PS-GRB.